An Intermediate Model of the Tropical Pacific Ocean*

BIN WANG AND TIANMING LI

Department of Meteorology, School of Ocean and Earth Science and Technology, University of Hawaii at Manoa, Honolulu, Hawaii

PING CHANG

Department of Oceanography, Texas A&M University, College Station, Texas

(Manuscript received 28 March 1994, in final form 22 August 1994)

ABSTRACT

An intermediate tropical Pacific Ocean model is developed to bridge the gap between anomaly models of El Niño and ocean general circulation models. The model contains essential physics for reproducing both the annual and interannual variations of sea surface temperature (SST). A new parameterization scheme for entrained water temperature is shown to work satisfactorily in both the cold tongues and warm pools. This scheme combines the Cane–Zebiak (CZ) model's dynamic framework and mixed layer physics, giving a more realistic description of the active tropical ocean.

Incorporation of the Niiler–Kraus scheme for turbulent entrainment enables the model to better simulate El Niño–Southern Oscillation in the central equatorial Pacific where the CZ model considerably underestimates observed SST variations. It also improves the model's performance on the seasonal cycle, especially in the central-eastern equatorial Pacific and the intertropical convergence zone (ITCZ). The potential energy generation induced by penetrative solar radiation tends to reduce entrainment in the central equatorial Pacific but to enhance mixing in the far eastern equatorial Pacific. Without this process, the model central (eastern) Pacific would be excessively cold (warm).

In response to an idealized sequential westerly burst located in the western equatorial Pacific, the CZ model produces SST oscillations in the eastern equatorial Pacific due to the thermocline oscillation associated with passages of Kelvin waves. In the present model, however, SST variation in the eastern Pacific is insignificant because local entrainment transcends the influence of thermocline oscillation; on the other hand, positive SST anomalies slowly amplify near the date line due to the reduction in wind-induced mixing and surface evaporation.

The annual variations of the oceanic momentum and heat transports associated with the annual march of the ITCZ are shown to have significant impacts on the annual mean state. On the other hand, including an annual mean heat flux correction in the present model does not strongly influence the amplitudes of annual and interannual SST variations. However, it does improve the phase structure of the annual cycle by providing a more accurate annual mean state.

1. Introduction

Sea surface temperature (SST) is a key variable in modeling earth's climate systems. In the last decade, a considerable number of upper-ocean models with a hierarchy of physical complexity have been developed to model tropical SST. Of those, models with an intermediate degree of complexity [termed intermediate models by McCreary and Anderson (1991)] have proven to be valuable for testing hypotheses such as Bjerknes' (1969) and for understanding the physics of the El Niño–Southern Oscillation (ENSO). They have even been used to predict El Niño with skill at lead times of several seasons (Cane et al. 1986).

The existing intermediate models of tropical ocean may be classified into two categories: Kraus–Turner (KT hereafter) model and Cane–Zebiak (CZ hereafter) model. The KT model is a one-dimensional bulk model of oceanic mixed layer (ML) first formulated by Kraus and Turner (1967) and successively implemented by many investigators (e.g., Niiler and Kraus 1977; Garwood 1977). It describes the vertical entrainment generated by wind stirring, convection, and other subgrid-scale processes. Turbulence is assumed to mix all the physical properties uniformly within the layer, and the integral properties of the ML (temperature, velocity,

to estimate entrainment rate in the thermodynamic equation. He examined the stability of the coupled ocean–atmosphere and obtained a comprehensive picture of various coupled unstable modes including those found by Philander et al. (1984). The KT model, however, could not determine entrained water temperature without invoking a proper dynamic framework or a multilayer model.

The CZ model originally designed by Cane (1979) for the study of wind-driven equatorial ocean circulation is a 1½-layer, linear, reduced gravity ocean coupled with a constant-depth surface layer. The model provides a simple yet extremely pertinent dynamic framework for modeling interannual variation of SST. The change in the model thermocline depth in response to a wind forcing captures an essential process of SST variation in the eastern equatorial Pacific during ENSO. The physics of the CZ model have been carefully analyzed (e.g., Cane and Zebiak 1985; Zebiak and Cane 1987; Battisti 1988; Neelin 1991; Jin and Neelin 1993). The model was also shown to be capable of reproducing reasonable SST seasonal variation (Seager et al. 1988, hereafter SZC model). In the western and central Pacific, however, the CZ model tends to underestimate SST anomalies (Cane 1993). The model also exhibits relatively large SST error along the eastern boundary of the Pacific Ocean in simulating SST climatology (Seager et al. 1988; Chang 1994), implying that coastal upwelling may not be handled properly. These shortcomings may be attributed to the neglect of entrainment: a fixed-depth surface layer does not allow a realistic specification of eastern boundary conditions nor a reliable assessment of SST in the regions where the thermocline is deep.

Chang (1994) assessed the performance of both models in simulating the annual cycle of SST in the tropical Pacific Ocean and found that both models have considerable skills in reproducing SST variability. However, he also noted that the CZ model has a bias toward dynamical responses to surface winds, whereas the KT model has a bias toward thermodynamic responses to surface heat fluxes.

Apparently, an integration of the complementary virtues of the two models is desirable. It is important for the CZ model to incorporate ML physics in the regions outside the equatorial cold SST tongues, where the effect of surface heat fluxes dominates that of oceanic advective processes. This motivates the development of the present model, which combines the dynamics of the CZ model with the ML physics of the KT model in a consistent and rudimentary manner and without a sizable increase in numerical computation. The present model differs from Schopf and Cane's (1983) 2½-layer model primarily in the treatment of the layer between the ML and the deep inert layer and in the parameterization of entrained water temperature as well as interfacial Reynolds stress. These are critical elements for integrating the virtues of the two models.

The goal of such a model development is, upon coupling an intermediate atmospheric model, to investigate the processes that govern the interaction between the annual and interannual variations and to explore the possibility of predicting ENSO without specifying annual cycle. For this purpose, the model must be capable of simulating both the annual cycle and interannual variation of the upper ocean. This is a challenge for an intermediate as well as a general circulation model (GCM), because certain physical processes on a seasonal timescale differ considerably from those on an ENSO timescale. Mitchell and Wallace (1992) first emphasized the important contribution of the positive feedback between the meridional wind component and the SST gradient to the annual variation of the cold tongue–ITCZ complexes in the Pacific and Atlantic Oceans. This process may not be critical to the ENSO cycle but is certainly relevant to the annual cycle in the Pacific. Wang (1994) showed that the annual cycle in the tropical eastern-central Pacific is alternatively dominated by a quasi-symmetric (with respect to the equator) equatorial-coastal mode, which primarily results from dynamic coupling of the ocean and atmosphere, and an antisymmetric monsoonal mode, which is driven by the contrast in surface heat fluxes between the Southern and Northern Hemispheres. The annual variation involves an interaction between the two modes. Chang and Philander's (1994) theoretical analysis of coupled ocean–atmosphere instability produced a family of antisymmetric and symmetric coupled ocean–atmosphere modes. They suggested that the antisymmetric mode may be instrumental in rapidly reestablishing the cold tongues during northern summer, whereas the symmetric mode contributes to the annual westward propagation of the near-equatorial zonal wind and SST.

In the next section we describe physical and numerical aspects of the model. Particular attention is given to the closure of the mixed layer equations, including parameterizations of entrained water temperature and interfacial momentum exchange. Section 3 presents a steady solution under the annual mean atmospheric forcing. To understand the model's response to atmospheric forcing, sensitivities of the steady solution to various processes are examined in section 4. Models with reduced physics are investigated and the linkage of the present model with the SZC model is discussed in section 5. Section 6 further elaborates differences between the SZC model and the present model in the processes that determine SST variation. The model's ability in reproducing annual cycle and interannual variations is demonstrated in section 7. The last section summarizes major results and discusses possible future improvements.

2. Formulation of the physical model

The thermal structure of the tropical Pacific Ocean (e.g., Fig. 2 of Wyrtki and Kilonsky 1984; Fig. 1 of

Seager et al. 1988) is characterized, to the lowest-order approximation, by an upper ML, a middle thermocline layer in which temperature drops rapidly with depth, and a lower abyss layer in which temperature is nearly a constant. On a timescale of a few years, the roles of

responding equations of motion in the s coordinates can be derived as follows:

$$\frac{\partial \tilde{h}}{\partial t} + \nabla_s \cdot (\tilde{h}\mathbf{V}) + \frac{\partial w_e}{\partial s} = 0, \qquad (2.3a)$$

ML base; $\mathscr{H}(W_e)$ is a Heaviside step function of W_e; and Q_0 and Q_{-h_1} are downward fluxes at the surface and the ML base, respectively. In derivation of (2.5b) it was assumed that the temperature in the thermocline layer decreases linearly from T_1 to T_r.

To predict $\mathbf{V}_1$, h_1, and T_1, the following variables must be determined: 1) thermocline depth h and the vertical shear $\mathbf{V}_s$; 2) entrainment velocity W_e and entrained water temperature T_e; 3) Reynolds stress at ocean surface τ_0 and at the ML base τ_{-h_1} and downward heat fluxes Q_0 and Q_{-h_1}.

b. Determination of the thermocline depth and shear flow

To determine thermocline depth, one may consider equations of motion governing the entire upper active ocean. To derive these equations, we use transformation:

$$s = \frac{z}{h}, \quad 0 \geqslant z \geqslant -h, \tag{2.6a}$$

so that the base of the thermocline becomes $s = -1$ in the s coordinates defined by (2.6a) and $\tilde{h} \equiv \partial z/\partial s = h$. The perturbation pressure is

$$P = \int_{-1}^{s} bh\,ds \approx h\bar{b}(s + 1), \tag{2.6b}$$

where $\bar{b}$ is the vertically averaged buoyancy. When the temperature in the thermocline layer decreases linearly from T_1 to T_r, $\bar{b}$ is related to b_1 by

$$\bar{b} = \frac{b_1}{2}\left(1 + \frac{h_1}{h}\right). \tag{2.6c}$$

Vertical integration of (2.3a, b) and use of (2.6a, b, c) yield

$$\frac{\partial h}{\partial t} + \nabla\cdot(h\mathbf{V}) = 0, \tag{2.7a}$$

$$\frac{\partial \mathbf{V}}{\partial t} + \mathbf{V}\cdot\nabla\mathbf{V} + f\mathbf{k}\times\mathbf{V} = -\nabla(\bar{b}h) + \frac{h}{2}\nabla\bar{b} + \frac{\tau_0}{\rho_r h} + \mu\nabla^2\mathbf{V}, \tag{2.7b}$$

where $\mathbf{V}$ is vertically averaged currents above the thermocline depth. The interfacial stress and the entrainment at $z = -h$ were neglected.

To estimate the vertical shear $\mathbf{V}_s$, we use the following approximation:

$$h\mathbf{V} = h_1\mathbf{V}_1 + h_2\mathbf{V}_2, \tag{2.8}$$

where $\mathbf{V}_2$ and h_2 are the vertically mean currents and thickness of the thermocline layer, respectively. In terms of $\mathbf{V}$ and $\mathbf{V}_1$, the shear

$$\mathbf{V}_s = \frac{h}{h - h_1}(\mathbf{V}_1 - \mathbf{V}). \tag{2.9}$$

c. Parameterization of the turbulent entrainment

A Kraus–Turner (Kraus and Turner 1967) type of oceanic ML is used to estimate entrainment rate (W_e). Niiler and Kraus (1977) gave a detailed derivation of W_e from the vertical integration of the steady turbulence-energy equation. If we neglect the production of turbulent energy by shear instability at the ML base, the equation for W_e reads

$$W_e\mathscr{H}(W_e)h_1\alpha g(T_1 - T_e) = 2m_s u_*^3 - \frac{h_1}{2}[(1 + m_b)B_0 - (1 - m_b)|B_0|] - \frac{\alpha g}{\rho_r c_w}\left(h_1 - \frac{2}{\gamma}\right)I_0, \tag{2.10}$$

where u_* is surface frictional velocity; the surface flux B_0 specifies the rate at which available potential energy is removed due to surface cooling: $B_0 = (\alpha g/\rho_r c_w)(Q_0 - I_0)$; $I_0 = (1 - R)F_{sw}$ is the flux of solar radiation penetration; $R = 0.55$ and $\gamma = 0.04$ m^{-1} (Ivanoff 1977) are the solar radiation penetration coefficient and an attenuation parameter, respectively; and F_{sw} is the downward solar radiation flux at the surface. The lhs term represents the rate of energy needed to agitate entrained water. In the rhs of (2.10), the first term denotes the rate of working by winds, and the second and third terms express the rate of potential energy generation by fluxes across the ocean surface and by solar radiation penetration, respectively. The effect of dissipation is included in the first two terms of the rhs of (2.10). The parameters m_s and m_b are turbulent mixing factors due to wind stirring and convection, respectively.

Equation (2.10) applies only when entrainment occurs ($W_e > 0$)—that is, the ML deepens. In the presence of strong radiational heating or weak winds, the wind stirring may be insufficient to produce entrainment. The ML must then become shallower until h_1 has decreased to a value that renders the rhs of (2.10) vanishing. The numerical treatment of the formation of a new ML is similar to that of Schopf and Cane (1983).

Parameterization of the temperature of entrained water is another key to the closure of the ML equations. Schopf and Cane (1983) tried to determine the entrained water temperature by imposing an additional constraint on the temperature discontinuity at the interface. The scheme was not very successful. Other schemes have been used in the previous studies (e.g., Seager et al. 1988; Chang 1994). In those schemes, the subsurface water temperature was determined using the emperical relations derived from observations. Although this may significantly improve the simulation, the models rely on some externally determined quantities and are not dynamically self-contained. Here we propose a simple dynamics-dependent parameterization scheme so that the scheme is self-contained. Consider a thin entrainment layer existing just below the

ML base (Fig. 1). This entrainment layer is a thin region of vigorous small-scale mixing, within which the turbulent flux drops sharply from a finite value to zero. Its thickness is denoted by Δh_e, which is a parameter. We further assume that the vertical temperature gradient in the entrainment layer may be estimated by the mean vertical temperature gradient in the thermocline layer, thus

$$T_1 - T_e = \Delta h_e \frac{T_1 - T_r}{h - h_1}. \tag{2.11}$$

d. Parameterization of Reynolds stresses and heat fluxes

The wind stress at the ocean surface is estimated by

$$\tau_0 = \rho_a C_D |\mathbf{V}_a| \mathbf{V}_a, \tag{2.12a}$$

where $\rho_a = 1.2$ kg m^{-3}, $C_D = 1.3 \times 10^{-3}$, and $\mathbf{V}_a$ is the surface wind. The dependence of vertical turbulent stress on depth is complicated and not precisely known. In the present model, two parameterization schemes were tested. The first assumes that vertical turbulent stress is a constant in a thin surface layer ($0 > z > -h_0$) and then decreases downward to zero at the thermocline depth according to a parabolic profile. Thus,

$$\tau_{-h_1} = \tau_0 \left(\frac{h - h_1}{h - h_0} \right)^2. \tag{2.12b}$$

The second scheme assumes that the interfacial stress at the ML base is $\tau_{-h_1} = \nu \partial \mathbf{V}/\partial z$, where ν is vertical eddy viscosity. Assume that across the ML base, the currents change by $\mathbf{V}_s$ on a characteristic vertical distance of h_1. Thus,

$$\tau_{-h_1} = \frac{\nu}{h_1} \mathbf{V}_s. \tag{2.12c}$$

The downward heat flux across the ocean surface is

$$Q_0 = F_{sw} - F_{lw} - F_l - F_s. \tag{2.13}$$

The solar shortwave flux F_{sw} is computed according to Berliand's (1952) formula:

$$F_{sw} = Q_s[1 - (a_1 + a_2 n)n](1 - A), \tag{2.14}$$

where Q_s is the monthly mean direct and diffuse maximum solar flux calculated from observation by Budyko and Miller (1974); n is monthly mean cloudiness; A is albedo with a value of 0.08 used over the ocean surface. Values for the coefficients a_1 and a_2 were tabulated in Table 4 of Budyko and Miller (1974). The effective longwave radiation flux is computed by

$$F_{lw} = \epsilon\sigma T_a^4 (0.39 - 0.05 e^{1/2})(1 - a_3 n^2) + 4\epsilon\sigma T_a^3 (T_1 - T_a), \tag{2.15}$$

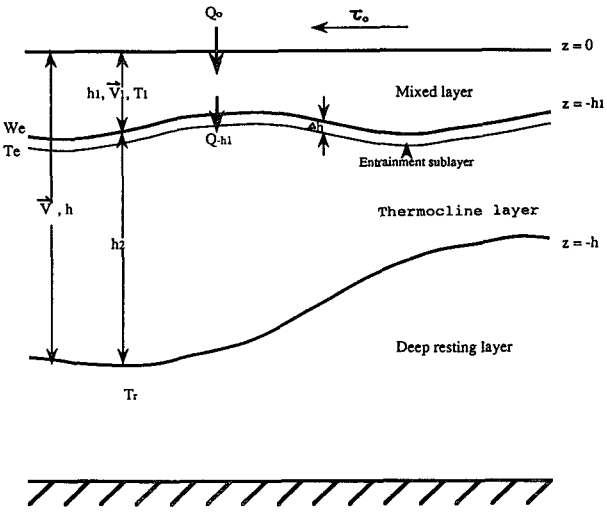

FIG. 1. Schematic diagram of the vertical structure of the model ocean. The surfaces $z = -h_1$ and $z = -h$ represent mixed layer base and thermocline depth, respectively. Both vary with time and space.

where T_a and e are, respectively, temperature and water vapor pressure (in mb) of the surface air; $\epsilon = 0.97$ is the infrared emissivity of the ocean; σ is the Stefan–Boltzman constant; and a_3 is a coefficient that varies with latitude in order to account for the variation of radiative properties of clouds with latitude (Table 9, Budyko and Miller 1974). The latent and sensible heat fluxes are calculated, respectively, by

$$F_l = \rho_a C_E L V (q_s - q_a) \tag{2.16}$$

$$F_s = \rho_a C_E C_p V (T_1 - T_a), \tag{2.17}$$

where $L = 2.5 \times 10^6$ J kg^{-1}, $C_p = 1004$ J kg^{-1} K^{-1}, and C_E is heat transfer coefficient. The saturation specific humidity q_s is a function of T_1 and can be calculated from the Claussius–Clapyron equation. The specific humidity (q_a) and temperature (T_a) of the surface air are determined from SST (i.e., T_1 in the model) by the following empirical relations:

$$q_a = [0.972 \times T_1(°\text{C}) - 8.92] \times 10^{-3}, \tag{2.18}$$

and

$$T_a = 1.03 T_1(°\text{C}) - 1.32. \tag{2.19}$$

Equations (2.18) and (2.19) are derived from monthly mean comprehensive ocean–atmosphere datasets (COADS) for a sample size over twenty thousands. The correlation coefficients are 0.99 and 0.96, respectively. In (2.16) and (2.17), V is surface wind speed. To account for effects of high frequency wind fluctuations on evaporation and to avoid the excessively high temperatures in regions of weak mean monthly winds (Philander et al. 1987), it is specified empirically by

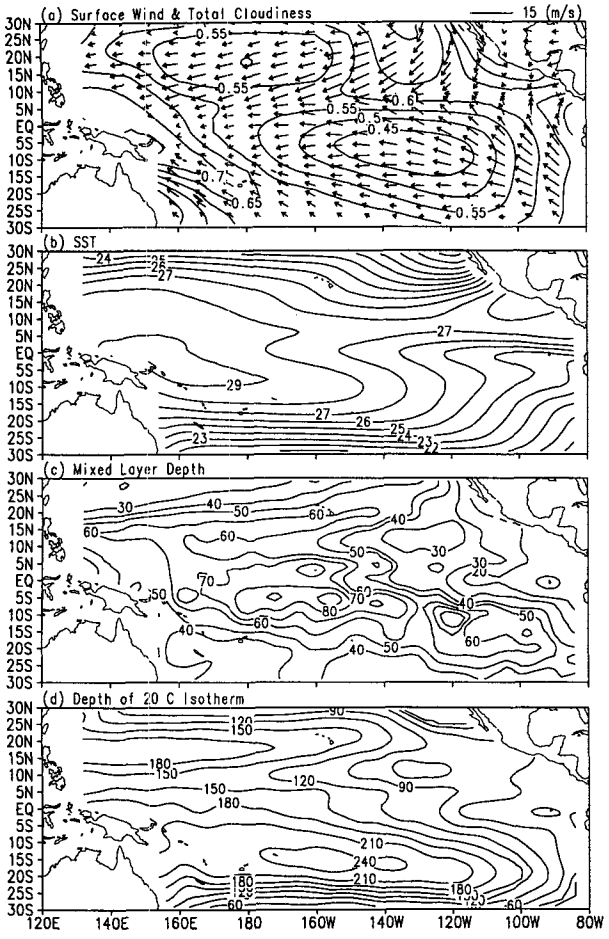

FIG. 2. Observed climatological annual mean fields of (a) surface winds and fractional total cloudiness, (b) sea surface temperature (°C), (c) mixed layer depth (m), and (d) the depth of the 20°C isotherm (m). The mixed layer depth (h_1) is defined as the depth at which the temperature is lower than SST by 0.5°C. The ocean temperature data are adopted from Levitus (1982). Surface winds and SST are from Sadler et al. (1987), and cloudiness is from Oberhuber (1988).

$$V = \begin{cases} |\mathbf{V}_a| & \text{if} \quad |\mathbf{V}_a| \geq 5 \text{ m s}^{-1} \\ 5 \text{ m s}^{-1} & \\ & \text{if} \quad 3 \text{ m s}^{-1} \leq |\mathbf{V}_a| \leq 5 \text{ m s}^{-1}. \\ |\mathbf{V}_a| + 2 \text{ m s}^{-1} & \text{if} \quad |\mathbf{V}_a| \leq 3 \text{ m s}^{-1} \end{cases} \tag{2.20}$$

The downward heat flux at the ML base is (Ivanoff 1977)

$$Q_{-h_1} = I_0 e^{-\gamma h_1}. \tag{2.21}$$

e. *Numerical methods and model parameters*

The model equations (2.5a–c) and (2.7a, b) along with (2.9a), (2.10), (2.11), (2.12a, b), and (2.13)–(2.21) are solved numerically using a finite-difference method similar to that used by Chang (1994). The Arakawa C grid (Arakawa and Lamb 1977) in a spherical coordinate is adopted. A potential entrophy conserving scheme is used for the momentum and mass equations and a density conserving form is employed in the heat equation to retain numerical accuracy (Bleck and Boudra 1981). The leapfrog scheme is used for time integration with a weak Robert smoothing coefficient of 0.005.

The model's domain extends from 120°E to 80°W, and 30°S to 30°N with a simplified description of the east and west boundaries of the Pacific Ocean. The standard spatial resolution of the model is 2° long by 1° lat, which requires an approximate time interval of 3 h. No-flux conditions for temperature and free-slip conditions for velocities are applied at the ocean boundaries. In addition, a large Rayleigh friction with a decay timescale of two days is used in narrow sponge layers at the northern and southern boundaries to eliminate artificial coastal Kelvin waves. The Rayleigh friction coefficients near the boundaries exponentially decay to zero toward the ocean interior. The most important parameters are listed in Table 1 along with their values used in the standard experiments.

3. Steady solution forced by long-term mean atmospheric forcing

To test the model's validity, a reference experiment was carried out using the full model described in section 2 with observed climatological annual mean surface winds compiled by Sadler et al. (1987) and cloudiness derived by Oberhuber (1988) from COADS as external forcing (Fig. 2a). The interfacial stress is described by Eq. (2.12b).

The time integration started from a resting ocean with a uniform SST of 30°C. A steady solution was reached nearly through the entire domain after about eight years of integration using the standard parameters listed in Table 1. A stronger viscosity results in a shorter spinup time (Chen et al. 1995). If a Rayleigh damping of a timescale of five months is added to the thermo-

TABLE 1. List of the model parameters and the standard values used in the reference experiment.

T_r	Reference temperature of the inert layer	10°C
R	Solar radiation penetration coefficient	0.55
G	Solar radiation attenuation coefficient	0.04 m^{-1}
C_D	Drag coefficient	1.3×10^{-3}
C_E	Moisture transfer coefficient	1.5×10^{-3}
h_0	Depth of constant-shear layer	10 m
M_s	Turbulent mixing coefficient due to wind stirring	1.25–0.4
m_b	Turbulent mixing coefficient due to convection	0.2
Δh_e	Thickness of the entrainment layer	5 m
μ	Horizontal turbulent momentum and heat diffusion coefficient	10^4 m^2 s^{-1}
r_h	Rayleigh damping coefficient for the thermocline depth equation	0
r	Rayleigh damping coefficient for the horizontal momentum equation	0

cline depth equation (2.7a), a steady state can be reached much sooner, in about 2 years. In the equatorial Pacific, the spinup time sensitively depends on the damping timescale for the thermocline depth.

The model-simulated steady-state ML temperature resembles closely climatological annual mean SST. For convenience, the simulated SST was displayed in Fig. 3a in terms of its difference from observed climatological mean SST shown in Fig. 2b. An excessively warm area is centered at 15°S, 135°W with a maximum error of 1.5°C. A major excessively cold area is found around 15°N, 140°W. Other areas of significant discrepancy are located in the middle of the cold tongue (5°S, 100°W) and the tropical portion of the South Pacific convergence zone (SPCZ). In comparison with the previous results of CZ and KT models (Chang 1994), the mean SST errors are reduced significantly in the ITCZ and equatorial cold tongue regions.

The simulated ML depth (Fig. 3b) and thermocline depth (Fig. 3c) bear qualitative resemblance to observed annual mean ML depth, defined as the depth at which the temperature differs from SST by one-half degree centigrade (Fig. 2c) and the depth of the 20°C isotherm (Fig. 2d), respectively. Major discrepancies between the simulated and above-defined observed ML depth occur in the tropical eastern North Pacific where the simulated ML depths were more than twice the observed values. The overall agreement between the model thermocline depth and observed depth of the 20°C isotherm is better than that between the modeled and the observed ML depths.

The simulated maximum speed of near-equatorial currents in the ML is about 50 cm s^{-1} in the central Pacific where the equatorial easterlies are strongest (Fig. 3b). This modeled South Equatorial Current (SEC) is confined between 3°N and 9°S in the eastern Pacific

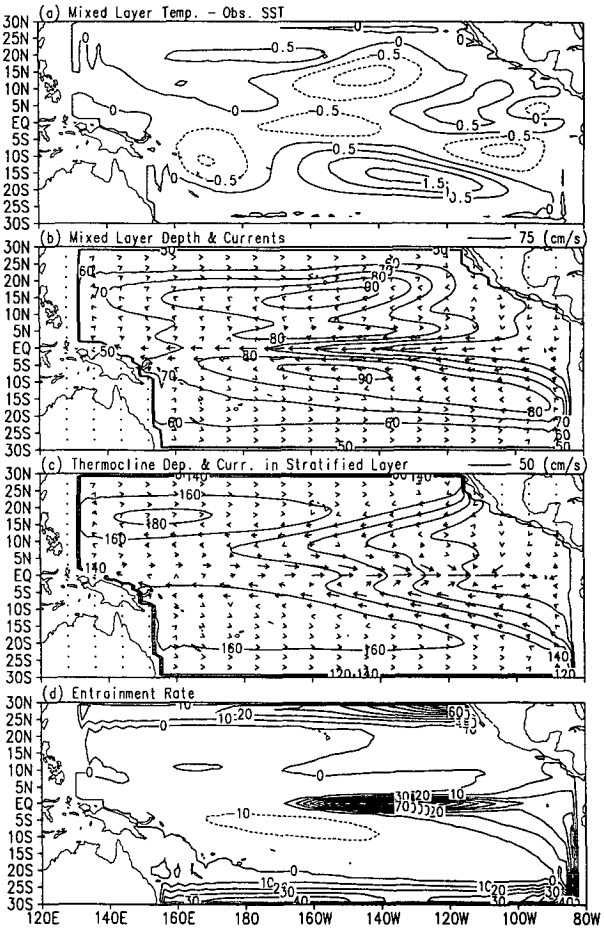

FIG. 3. Model-simulated steady solution forced by observed climatological annual mean surface winds, cloudiness, and solar radiation in the reference experiment: (a) mixed layer temperature minus observed annual mean SST (°C); (b) mixed layer depth h_1 (m) (con-

The present model has two specific features in the usage of bulk aerodynamic formula (2.16). First, the humidity of the surface air was determined from SST using an empirical relation, (2.18). The physical basis for this relation is that the air humidity over the open ocean is constantly adjusted toward a quasi-equilibrium state with SST via surface evaporation and turbulent mixing. As such, the surface air humidity follows SST closely on timescales longer than a month. Our experiments indicate that the latent heat flux computed using (2.18) is nearly the same as that computed using observed surface air humidity. The use of (2.18), therefore, not only provides satisfactory results, but also removes the dependence of the ocean model on atmospheric humidity being an external forcing. When the ocean model is coupled with an atmospheric model, the coupled model will not suffer from the inaccuracy arising from the model-computed surface moisture parameter. Secondly, following Philander et al. (1987), we used a modified monthly mean wind speed, (2.20), in computing latent and sensible heat fluxes. Equation (2.20) is derived empirically through a careful comparison of a series of controlled experiments. Without such a parameterization, excessive high temperature would occur in the warm pool regions where wind speed is small and ocean dynamical processes do not play an important role in SST variation.

b. *Entrainment rate*

The importance of the entrainment associated with various processes (wind stirring, convection, potential energy generation due to penetrative radiation, and background dissipation) was assessed through controlled experiments.

The turbulent mixing associated with a decrease in potential energy generation due to an increase in penetrated solar radiation [the third term in the rhs of (2.10)] was found to play a significant role in the ML heat balance in the equatorial Pacific. This process enhances (reduces) entrainment where the ML is relatively shallow (deep). Without this process, the far eastern equatorial Pacific would be excessively warm, because the ML is overstabilized by the excessive surface heat fluxes and the entrainment was underestimated; on the other hand, the equatorial central Pacific would be excessively cold due to strong wind stirring and insufficient stabilization by thermal stratification. Inclusion of this process leads to an improved simulation in the ML temperature in the eastern-central equatorial Pacific. This process also tends to reduce the entrainment rate in the subtropics.

The value for the wind stirring factor m_s was determined to be 1.25 by laboratory experiments (Niiler and Kraus 1977) but can vary in a wide range from 0.4 to 8 based on oceanic observations (Garett et al. 1979). In general, increasing m_s enhances the entrainment rate, favoring ML cooling. The influence of m_s on the ML depth depends on latitude. In the equatorial region where the ML depth is controlled by ocean dynamics, it is not sensitive to the change in the wind stirring factor m_s. In the subtropics, however, the ML depth sensitively increases with increasing m_s. The opposing effects of increasing entrainment rate and increasing ML depth on the ML temperature tend to cancel each other. As a result, the ML temperature is not sensitive to changes of m_s. In the present model we used a latitude-dependent value: m_s decreases linearly from 1.25 at the equator to 0.4 at 30° latitude.

The turbulent coefficient associated with convection, m_b, is taken as a constant, $m_b = 0.2$, according to Gaspar (1988). Changing of m_b from 0.2 to 0.4 altered the ML depth only in the subtropics; little change was observed in the ML temperature. The solution is also not sensitive to changes in solar radiation penetration and attenuation parameters. Introduction of a background dissipation (Kim 1976) in (2.10) results in a larger (smaller) reduction of W_e in the regions having a deeper (shallower) ML. But in general, the effect is not essential. The present model excluded the background dissipation.

c. *Entrained water temperature and the reference temperature*

The parameterization of T_e, Eq. (2.11), requires a specification of the entrainment layer thickness. A thicker entrainment layer implies a larger $T_1 - T_e$ and a stronger cooling in the presence of entrainment. When the entrainment layer thickness doubles (from 5 to 10 m), the ML temperature decreases by 0.5°–2.0°C in the regions where the entrainment rate is large and/or the thermocline layer is thinner (Fig. 4a). Dramatic decreases of ML temperature (more than 2°C)

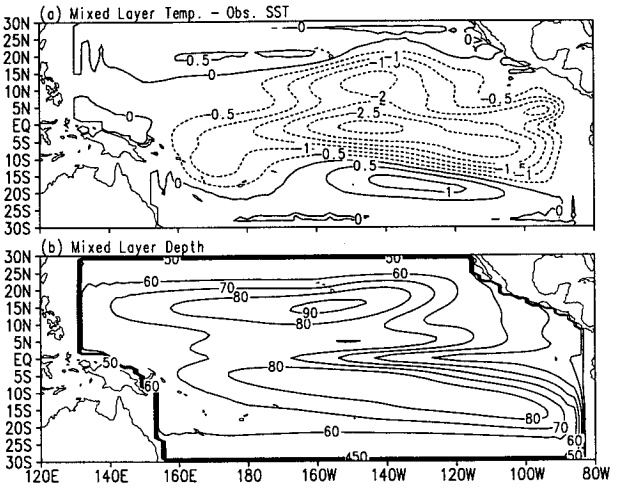

FIG. 4. (a) As in Fig. 3a, and (b) mixed layer depth h_1 (m) as in Fig. 3b except for the experiment with an increased entrainment sublayer thickness $\Delta h_e = 10$ m.

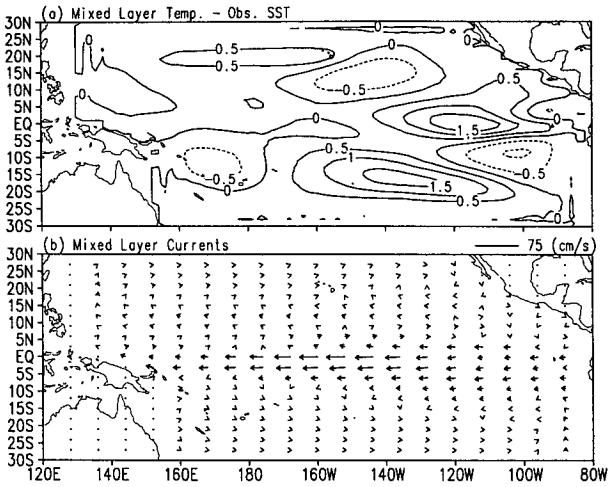

FIG. 5. (a) As in Fig. 3a, and (b) the vertical mean currents in the mixed layer as in Fig. 3b except for the experiment with an alternative parameterization scheme for interfacial stress, Eq. (2.12c).

are found in the central and eastern equatorial Pacific (110°–150°W) where the thermocline layer is thin and the ML is shallow (Fig. 4b). In the areas where entrainment is absent or the thermocline layer is thick, the ML temperature is either not affected or is little affected by this parameter. The changes in the entrainment layer thickness have little influence on the ML and thermocline depths and currents.

The choice of the reference temperature T_r also affects the entrained water temperature [Eq. (2.11)]. It degree, except in the eastern equatorial Pacific around 120°W where the difference reaches 0.5°–1.0°C (Figs. 5a and 3a). The ML and thermocline depths are not affected appreciably by changing the interfacial stress parameterization. The patterns of currents and entrainment velocity are also very similar. The primary impact of using (2.12c) is the reduction in the strength of the equatorial currents in the ML (Fig. 5b) and the thermocline layer (figure not shown), especially in the eastern equatorial Pacific. This is due to the reduction in the wind forcing in the ML when (2.12c) is used. As a result of weakening in the momentum input into the ML, the entrainment rate reduces by about 25% and SST increases in the eastern equatorial Pacific. When a smaller vertical turbulent coefficient of 20 $cm^2\ s^{-2}$ was used in (2.12c), the currents and entrainment rates increased. As such, the solution was nearly the same as that of the reference run. This indicates that the two parameterization schemes may yield comparable solutions if a proper value for eddy viscosity in (2.12c) is used. Additional experiments showed that neglect of the interfacial stress at the thermocline layer base has little effect on the solution.

e. Background Rayleigh damping

The Rayleigh damping for the thickness of the upper active ocean or thermocline depth has considerable impacts on the equatorial dynamics. To demonstrate these impacts, we conducted an experiment in which a Rayleigh damping is added in (2.7a). The damping

particular, the meridional pressure gradient force in the vicinity of the equator reversed its direction, resulting in a fictitious westward equatorial undercurrent. The direction reversal in the thermocline layer, in turn, reduces the drag to the ML currents, causing a marked acceleration of the ML currents (figure not shown).

The ML depth, however, was not affected noticeably. The deepening of the thermocline base in the eastern Pacific results in a thickening of the thermocline layer and a corresponding increase in the entrained water temperature [see (2.11)]. As a result, the ML temperature was increased by about 0.5°C in the eastern Pacific (Fig. 6a). Meanwhile, the ML temperature was reduced by about 0.5°C in the western equatorial Pacific due to increased westward advection of cold water.

Rayleigh damping on momentum and mass was not used in the present model. Second-order horizontal momentum and heat diffusions are included with a coefficient of 10^8 cm^2 s^{-1}. This is used for suppressing small-scale computational noise. A by-product of the momentum diffusion might be a weakening of the equatorial currents. It, however, has little effect on the entrainment rate and the ML temperature.

5. Models with reduced physics

A simplified version that is similar to the SZC model can be obtained from the full model (hereafter model A) described by Eqs. (2.5a–c), (2.7a, b), and (2.10) with (2.12c) by introducing the following assumptions or simplifications.

1) The ML depth is constant—that is, $h_1 = H_1$. In this case, the entrainment rate is identical to an upwelling rate and is determined, from (2.1b), by the vertical integrated divergence in the ML:

$$W_s = H_1 \nabla \cdot \mathbf{V}_1. \tag{5.1}$$

2) The pressure gradient force induced by the horizontal gradients of buoyancy force in the upper active ocean is neglected; that is, $b_1 = b = \text{const}$.

3) The momentum equations, (2.5b) and (2.7b), and the thermocline depth equation (2.7a) are linearized as

$$\frac{\partial \mathbf{V}_1}{\partial t} + f\mathbf{k} \times \mathbf{V}_1 = -b\nabla h' - \frac{|W_s|}{H_1}\mathbf{V}_s + \frac{1}{\rho_r H_1}(\tau_0 - \tau_{-h_1}) + \mu\nabla^2\mathbf{V}, \tag{5.2a}$$

$$\frac{\partial \mathbf{V}}{\partial t} + f\mathbf{k} \times \mathbf{V} = -b\nabla h' + \frac{\tau_0}{\rho_r H} + \mu\nabla^2\mathbf{V}, \tag{5.2b}$$

$$\frac{\partial h'}{\partial t} + H\nabla \cdot \mathbf{V} = 0. \tag{5.2c}$$

4) The drag at the ML base due to interfacial stress and the turbulent momentum exchange associated with entrainment can be simply expressed by a Rayleigh damping, $-r_s\mathbf{V}_s$, where

$$r_s = \frac{|W_s|}{H_1} + \frac{\nu}{H_1^2}. \tag{5.3}$$

5) A Rayleigh damping is applied to the perturbation thermocline depth equation.

With the above simplifications, the governing equations (2.5b, c) and (2.7a, b) become

$$\frac{\partial \mathbf{V}_1}{\partial t} + f\mathbf{k} \times \mathbf{V}_1 = -b\nabla h' + \frac{\tau_0}{\rho_r H_1} - \frac{H - H_1}{H} r_s \mathbf{V}_s, \tag{5.4a}$$

$$\frac{\partial T_1}{\partial t} + \mathbf{V}_1 \cdot \nabla T_1 = -\frac{W_s}{H}\mathscr{H}(W_s)(T_1 - T_e) + \frac{Q_0 - Q_{-h_1}}{\rho_r C_w H_1} + \mu\nabla^2 T_1, \tag{5.4b}$$

$$\frac{\partial h'}{\partial t} + H\nabla \cdot \mathbf{V} = 0, \tag{5.4c}$$

$$\frac{\partial \mathbf{V}}{\partial t} + f\mathbf{k} \times \mathbf{V} = -b\nabla h' + \frac{\tau_0}{\rho_r H}, \tag{5.4d}$$

where $h' = h - H$ is perturbation thermocline depth, and

$$\mathbf{V}_s = \frac{H}{H - H_1}(\mathbf{V}_1 - \mathbf{V}) \tag{5.5}$$

is proportional to the vertical shear between the ML and thermocline layer. Using (5.5), Eqs. (5.1) and (5.4a) can be casted into the following forms

$$W_s = H_1 \nabla \cdot \mathbf{V} + \frac{H_1(H - H_1)}{H}\nabla \cdot \mathbf{V}_s, \tag{5.6a}$$

$$\frac{\partial \mathbf{V}_s}{\partial t} + f\mathbf{k} \times \mathbf{V}_s = \frac{\tau_0}{\rho_r H} - r_s\mathbf{V}_s + \mu\nabla^2\mathbf{V}_s. \tag{5.6b}$$

The governing equations (5.6a, b) and (5.4b, c, d) are basically the same as the SZC model. This simplified model is referred to as model B. It should be pointed out that model B is not equivalent to the SZC model. There are two major differences. One is the treatment of latent and sensible heat fluxes. The other lies in the parameterization of the subsurface water temperature. In the SZC model the subsurface water temperature is a critical parameter and is determined using an empirical relation derived from observations. Although this is not a self-contained scheme, it may significantly improve the simulation of the SST variation. In view of the differences between the model B and the SZC model, the comparison of model A and model B should not be understood as a comparison of the performance between the present model and the SZC model.

To investigate the roles of various processes in the dynamics and thermodynamics of the tropical upper

ocean, model A was systematically distilled to model B by adopting each of the above-listed simplifications at each step. A family of intermediate reduced-physics models were obtained. Experiments with these models were performed using exactly the same forcing and parameters as those used in the control run. The intent was to examine impacts of various assumptions and simplifications.

With the first assumption, $H_1 = 50$ m, the resulting ML temperature in the eastern-central equatorial Pacific is about 4°C colder than that in the control run, because the wind stress acting on the ML water column increased drastically due to the fixation of the ML depth. When simplifications 2 and 3 are further adopted, the heat balance is severely damaged so that no reasonable solution can be obtained. If the simplifications 1–4 are used as a group, however, a reasonable ML temperature field may result if a sufficiently large Rayleigh friction coefficient r_s (corresponding to a damping timescale on an order of one day) is used. In the SZC model, strong Rayleigh damping is needed for maintaining a balance with surface wind stress and the Coriolis force so that a desirable wind-driven frictional transport or upwelling rate can be obtained. It is concluded that assumptions 1–4 should be used as a group when the model A is simplified.

Figure 7 shows the steady solution produced by model B under annual mean forcing. In comparison with the steady solutions of model A (Fig. 3), the ML temperature in model B shows larger errors ranging from −1.4° to 2.0°C; and the ML currents are substantially weaker, especially in the eastern and central equatorial Pacific. The SST error pattern is similar to that shown by Fig. 3 of Chang (1994). The equatorial undercurrents in the thermocline layer have a wrong direction in model B due to the use of assumption 5 listed previously. Comparison of results obtained from models A and B suggests that some physical processes

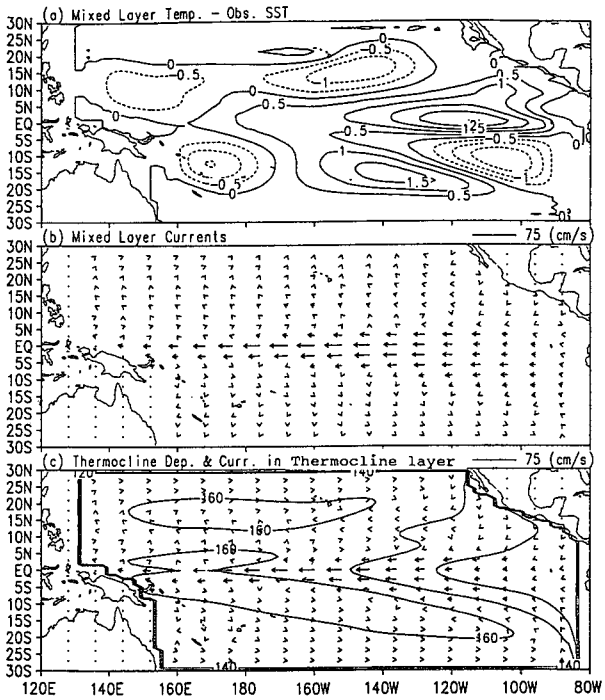

FIG. 7. (a) As in Fig. 3a, (b) the vertical mean currents in the mixed layer as in Fig. 3b, and (c) as in Fig. 3c except for the solution obtained using simplified model B.

(advection by currents, upwelling or entrainment, etc.) affecting SST in the two models are quite different. We will further elaborate this point in the next section.

6. Transient response

After the mean states were obtained using climatological annual mean forcing, a transient wind forcing was added to the mean surface wind, which has a stationary Kelvin wavelike structure centered at 150°E with an amplitude oscillating with a period of 30 days:

$$U = U_0 \cos[\pi(x - 150)/L_x] \times \exp[(y/L_y)^2] H[\sin(2\pi t/T)], \quad (6.1)$$

where $U_0 = 8$ m s^{-1}, 130°E $< x <$ 170°E, $T = 30$ days, $L_x = 40°$ long, $L_y = 10°$ lat, and H is a Heaviside function of $\sin(2\pi t/T)$. The transient response was obtained by subtracting the model mean state from the time-dependent solution forced by the total winds (mean plus transient winds).

In response to the transient wind forcing (6.1), both models show clear signals of Kelvin waves in thermocline depth fluctuation. These Kelvin waves are excited by the stationary wind fluctuation in the western equatorial Pacific. They propagate eastward across the entire Pacific basin as free modes, causing periodic fluctuations of the thermocline depth in the eastern Pacific. This indicates that the two models have similar dynamics: The thermocline is nearly in a Sverdrup balance with surface wind stress in the forcing region, and the periodic fluctuation in wind stress induces regular oscillations in the thermocline depth which, in turn, initiate free internal Kelvin waves.

The responses of SST in the two models, however, differ considerably (Fig. 8). In model A, major positive temperature anomalies amplify with time in the western Pacific centered at 170°E with a maximum of 0.35°C occurring around day 80 (Fig. 8a). The positive anomalies in the eastern Pacific, on the other hand, are rather weak. In contrast, in model B, the largest positive temperature anomalies appear in the eastern Pacific around 100°W, whereas the positive temperature anomalies around 170°E are modest (Fig. 8b).

The different SST responses in the two models result from different ML physics. In the eastern Pacific where the thermocline is shallow, the surface-layer temperature in model B is primarily controlled by the strength of upwelling and the vertical temperature gradient in the thermocline layer. The Ekman pumping–induced

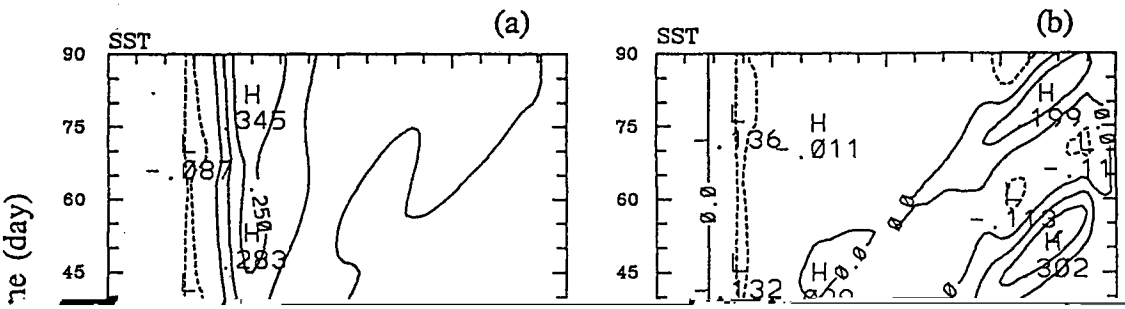
(a)
SST
90
75
60
45
H
.345
-.087
.250
.283
(b)
SST
90
75
60
45
.136
H
.011
H
.199
-.113
H
.302
.132

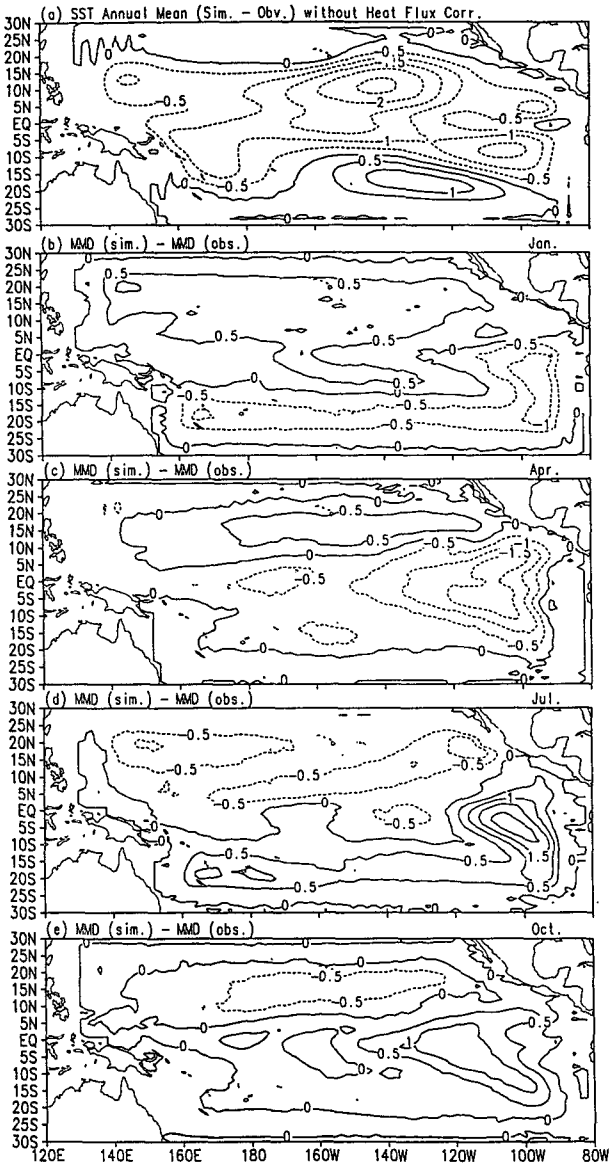

FIG. 9. Differences between the model-simulated ML temperature and observed SST (simulation-observation) for annual mean (a) and monthly mean departures of January (b), April (c), July (d), and October (e). The simulation was performed using climatological annual-cycle forcing of surface winds, cloudiness, and insolation.

decreases are in the latitude belt between the equator and 15°N. The difference between Fig. 9a and Fig. 3a is attributed to the nonlinear effects of the transient annual variation on the time-mean flow. The annual variations are strongest in the latitude band between the equator and 15°N, because the annual variation of the wind forcing and cloudiness are strongest in this region due to the annual north–south migration of the ITCZ.

Subtracting the model annual mean from the equilibrium annual cycle yields an annual monthly mean departure of SST. The differences in monthly mean departures between the simulated ML temperature and observed SST are shown in Figs. 9b–e. In the subtropics, the simulated departure in the winter (summer) hemisphere is higher (lower) than its observed counterpart. This systematic error is due to the fact that the amplitude of the simulated annual variation is smaller than that observed. In the eastern equatorial Pacific, the simulated annual variation is dominated by an annual harmonic regardless of the dominant semi-annual solar radiational forcing. This agrees with observations. Errors, however, are the largest in the eastern equatorial Pacific. These errors result primarily from a phase delay in the simulated seasonal transition. Around 110°W the simulated seasonal transition lags observation by 1 to 2 months. The exact cause for the phase delay is unknown. Several factors may contribute to it, among which the errors in the simulated ML depth, the neglect of higher vertical modes, and the uncertainty in the calculation of the surface heat fluxes can be major contributors.

One of the remedies to reduce the uncertainty in estimating surface heat fluxes is to modify the net surface heat flux term Q_o by adding a correction:

$$Q_o^* = Q_o - k(T_1 - T_*), \qquad (7.1)$$

where Q_o^* is the corrected surface heat flux and T_* is the observed climatological annual mean SST. The heat flux correction takes a Newtonian damping form that relaxes predicted ML temperature T_1 toward T_*. A value of 35 (W m^{-2} K^{-1}) for the coefficient k was taken in the previous GCM studies (e.g., Gordon and Corry 1991) and intermediate models (Chang 1994), which is equivalent to a relaxation time of approximately 2 months. The present model adopted a smaller correction coefficient that corresponds to a relaxation time of 5 months.

It is important to note that the inclusion of an annual mean heat flux correction does not affect the depths of ML and thermocline layer and the currents (figure not shown). It also does not significantly reduce the amplitudes of the SST annual cycle. The simulated annual cycle with the mean heat flux correction exhibits a better agreement with observed annual cycle in the eastern equatorial Pacific (Figs. 10b–e). The roles of the heat flux correction are twofold. On one hand, it effectively adjusts the model's long-term mean toward observed value, yielding a much improved annual mean field (Fig. 10a). On the other hand, by producing a more accurate annual mean state, it also reduces (but does not necessarily eliminate) the phase delay of the annual cycle in the eastern equatorial Pacific. Because the mean heat flux correction does not significantly reduce the amplitude of the annual cycle, it should not significantly affect the model ENSO signal, as will be demonstrated in the next subsection.

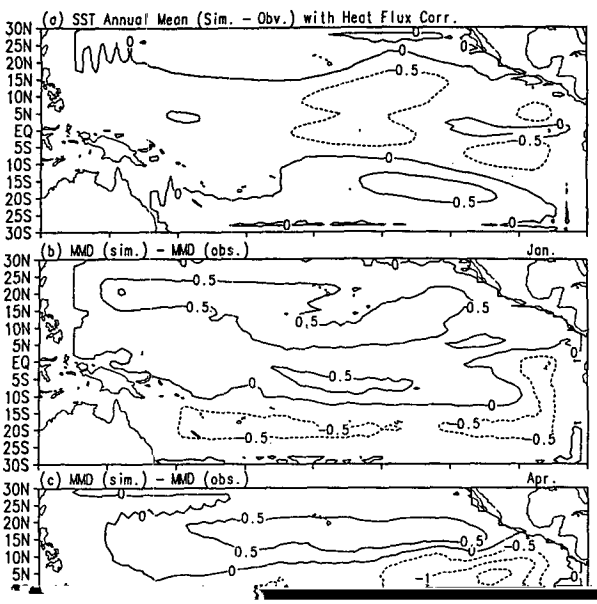

monthly mean observations. All other parameters are the same as in the reference experiment. An annual mean heat flux correction was included with a relaxation time of five months. The model integration started from January climatology generated using annual cycle forcing. An additional 1-year forcing was padded to the forcing field prior to January 1964 during which the wind forcing was gradually changed from the climatological January mean to the mean of January 1964. The anomalous fields were obtained by subtracting the model annual cycle from the full time-dependent solution. In the simulation, the ML temperature was damped to observed climatological monthly mean SST at the northern and southern boundaries, but there was no such damping at the eastern and western boundaries.

Figure 11a displays modeled anomalous ML temperature along the equator as a function of time. Major El Niños (1965, 1972, 1982/83, 1986/87) and moderate El Niños (1969, 1976) are all well captured except

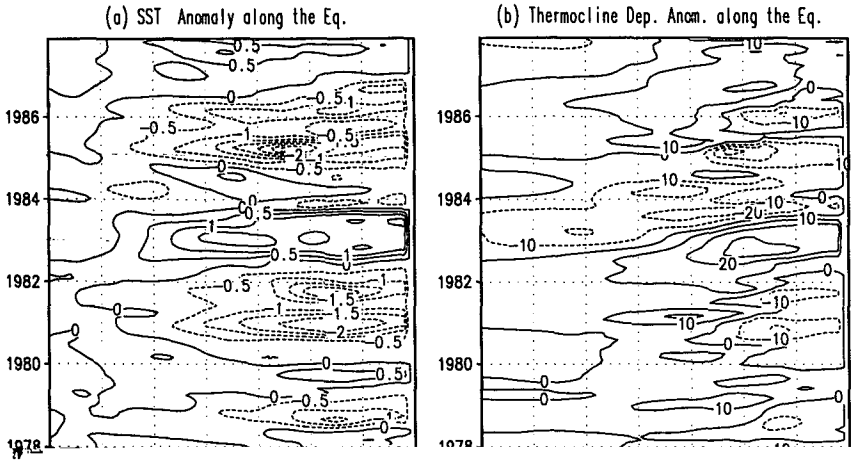
(a) SST Anomaly along the Eq.
(b) Thermocline Dep. Anom. along the Eq.
1986
1984
1982
1980

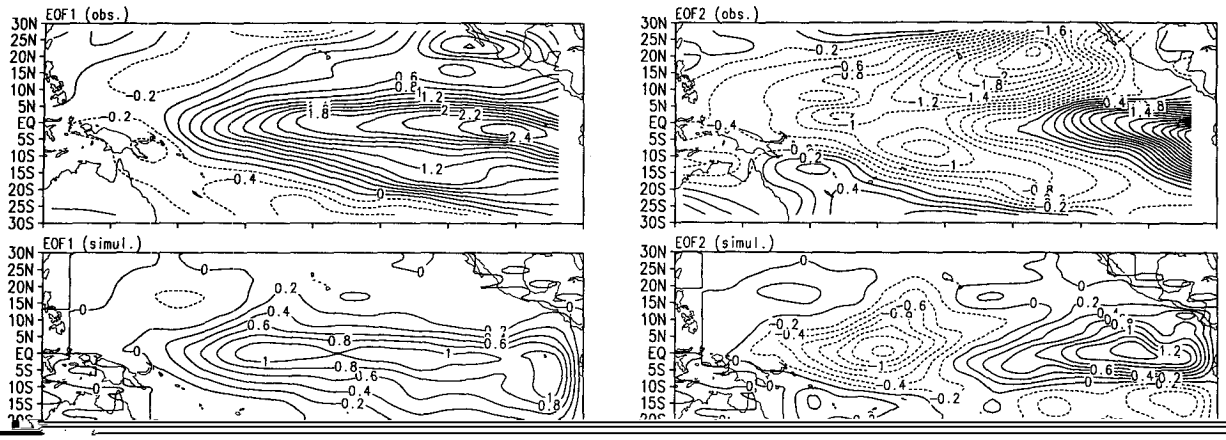
EOF1 (obs.)
EOF2 (obs.)
EOF1 (simul.)
EOF2 (simul.)
30N
25N
20N
15N
10N
5N
EQ
5S
10S
15S
20S
25S
30S

the resultant ML temperature fields are almost the same. This approach will avoid errors possibly arising from the use of atmospheric model-computed air humidity and temperature when coupling the ocean model with an atmospheric model.

The solution in the present model, thus, depends upon only two atmospheric variables: surface winds and cloud cover for given insolation. The surface winds affect ML temperature indirectly by changing entrained water temperature as discussed early in this section. More importantly, the surface winds can affect ML temperature by directly changing the turbulent entrainment, the surface evaporation and sensible heat flux, and the temperature advection by wind-induced currents. The cloudiness influences ML temperature via directly changing shortwave and longwave radiation fluxes and indirectly changing the entrainment rate associated with the mixing process.

The change in ML temperature is thus a result of subtle balance and complex interaction among the above-mentioned processes. As such, the response of SST to a transient wind forcing in the present model differs considerably from the SZC model in which the turbulent mixing is absent. For a given stationary wind forcing of intraseasonal oscillation located in the western equatorial Pacific, for instance, the SZC model shows a decaying oscillation in SST that is most prominent in the remote eastern Pacific, whereas the present model exhibits a slow amplification of positive SST anomalies just to the east of the forcing. Observations have shown considerable intraseasonal variations in the sea level height and the thermocline depth, which are remotely forced by the counterpart variations in surface winds over the western equatorial Pacific (e.g., Ericksen et al. 1983; Enfield 1987). The SST, however, does not seem to have significant response in the eastern Pacific. In the ocean GCM experiment (Latif et al. 1988) westerly bursts in the western Pacific (130°–ENSO variability in the central equatorial Pacific where the CZ model substantially underestimates SST anomalies.

Numerical experiments demonstrated that the momentum and heat transports during the annual cycle can significantly modify the annual mean ML temperature and the depths of the thermocline and ML. The transient effect tends to lower the annual mean SST in the tropical Pacific Ocean by 0.5°–1.5°C. It is most significant in the vicinity of the ITCZ, which migrates annually back and forth between 4° and 12°N.

The most serious problem with modeling the annual cycle of SST is the phase delay. This problem is likely related to the uncertainty in the surface heat flux forcing (in particular, the cloud effects on solar radiation) and model errors in representing ML processes. At this stage, an effective way to leverage the problem is to introduce a correction to the long-term mean heat flux. This approach was previously used in GCM simulations (e.g., Meehl et al. 1985; Han 1984; Gordon and Corry 1991) and intermediate models (e.g., Chang 1994). We have shown that the inclusion of a mean heat flux correction in the present model does not significantly influence amplitudes of the annual and interannual variations of ML temperature. It, however, significantly improves the simulation of the annual cycle by providing a more accurate mean state.

The tests of the present model in reproducing SST variabilities on various timescales are preliminary. Further analyses are needed to diagnose the causes of the model's major deficiencies. Inclusion of the effects of stratocumulus clouds on solar radiation appears to be desirable for further improvement. The mechanisms of ML temperature variability need to be better understood before coupling atmospheric models.

Acknowledgments. We thank Mr. Yan Wang for his assistance. Drs. J. M. Oberhuber and X. Wang kindly provided cloudiness and COADS data that were used

——, and A. C. Hirst, 1989: Interannual variability in the tropical atmosphere/ocean system: Influence of the basic state, ocean

Latif, M., and N. E. Graham, 1992: How much predictive skill is contained in the thermal structure of an OGCM? *J. Phys.*

Berliand, M. E., and T. G. Berliard, 1952: Determining the net longwave radiation of the earth with the consideration of the effect of cloudiness (in Russian). *Izv. Akad. Nauk. SSSR, Ser. Geofiz.*, **1**.

Bjerknes, J., 1969: Atmospheric teleconnections from the equatorial Pacific. *Mon. Wea. Rev.*, **97**, 526–535.

Bleck, R., and D. B. Boudra, 1981: Initial testing of a numerical ocean circulation model using a hybrid (quasi-isopicnic) vertical coordinate. *J. Phys. Oceanogr.*, **11**, 755–770.

Budyko, M. I., and D. H. Miller, 1974: *Climate and Life.* Academic Press, 508 pp.

Cane, M. A., 1979: The response of an equatorial ocean to simple wind stress pattern. Part I: Model formulation and analytical results. *J. Mar. Res.*, **37**, 233–252.

——, 1993: Tropical Pacific ENSO models: ENSO as a mode of the coupled system. *Climate System Modeling,* K. E. Trenberth, Ed., Cambridge University Press, 788 pp.

——, and S. E. Zebiak, 1985: A theory for El Niño and the Southern Oscillation. *Science,* **228**, 1084–1087.

——, ——, and S. C. Dolan, 1986: Experimental forecasts of El Niño. *Nature,* **321**, 827–832.

Chang, P., 1994: A study of seasonal cycle of sea surface temperature in the tropical Pacific Ocean using reduced gravity models. *J. Geophys. Res.*, in press.

——, and S. G. Philander, 1994: A coupled ocean–atmosphere instability of relevance to the seasonal cycle. *J. Atmos. Sci.*, **51**, 3627–3648.

Chao, Y., and S. G. H. Philander, 1993: On the structure of the Southern Oscillation. *J. Climate,* **6**, 450–469.

Chen, Y.-Q., D. S. Battisti, and E. S. Sarachik, 1995: A new ocean model for studying the tropical oceanic aspects of ENSO. *J. Phys. Oceanogr.*, **25**, in press.

Enfield, D., 1987: The intraseasonal oscillation in eastern Pacific sea levels: How is it forced? *J. Phys. Oceanogr.*, **17**, 1860–1876.

Ericksen, C. C., M. B. Blumenthal, S. P. Hayes, and P. Ripa, 1983: Wind-generated equatorial Kelvin waves observed across the Pacific Ocean. *J. Phys. Oceanogr.*, **13**, 1622–1640.

Garett, A. E., T. B. Stanford, and T. R. Osborn, 1979: Surface mixing layers in the Sargasso Sea. *J. Phys. Oceanogr.*, **7**, 455–468.

Garwood, R. W., 1977: An oceanic mixed layer model capable of

Levitus, S., 1982: Climatological atlas of the World Ocean. NOAA Prof. Paper, 13, U.S. Dept. of Commerce, Washington, D.C.

McCreary, J. P., and D. L. T. Anderson, 1991: An overview of coupled ocean–atmosphere models of El Niño and the Southern Oscillation. *J. Geophys. Res.*, **96**, 3125–3150.

Meehl, G. A., W. M. Washington, and A. J. Semtner, 1985: Experiments with a global ocean model driven by observed atmospheric forcing. *J. Phys. Oceanogr.*, **15**, 92–104.

Mitchell, T. P., and J. M. Wallace, 1992: The annual cycle in equatorial convection and sea surface temperature. *J. Climate,* **5**, 1140–1156.

Neelin, J. D., 1991: The slow sea surface temperature mode and the fast-wave limit: Analytic theory for tropical interannual oscillations and experiments in a hybrid coupled model. *J. Atmos. Sci.*, **48**, 584–607.

——, M. Latif, and F.-F. Jin, 1994: Dynamics of coupled ocean–atmosphere models: The tropical problem. *Annu. Rev. Fluid Mech.*, **26**, 617–659.

Niiler, P. P., and E. B. Kraus, 1977: One-dimensional models of upper ocean. *Modeling and Prediction of the Upper Layers of the Ocean.* E. B. Kraus, Ed., Pergamon Press, 143–172.

Oberhuber, J. M., 1988: An atlas based on the "COADS" data set: The budget of heat, buoyancy and turbulent kinetic energy at the surface of the global ocean. Max-Planck Institut für Meteorologie, Report No. 15, 196 pp.

——, W. J. Hurlin, and A. D. Seigel, 1987: Simulation of the seasonal cycle of the tropical Pacific Ocean. *J. Phys. Oceanogr.*, **17**, 1986–2002.

Philander, S. G. H., and R. C. Pacanowski, 1986a: A model of seasonal cycle in the tropical Atlantic Ocean. *J. Geophys. Res.*, **91**, 14 192–14 206.

——, and ——, 1986b: The mass and heat budget in a model of the tropical Atlantic Ocean. *J. Geophys. Res.*, **91**, 14 212–14 220.

——, T. Yamagata, and R. C. Pacanowski, 1984: Unstable air–sea interaction in the Tropics. *J. Atmos. Sci.*, **41**, 604–613.

Sadler, J. C., M. A. Lander, A. M. Hori, and L. K. Oda, 1987: Tropical marine climate atlas. Vol. 1, Pacific Ocean. Report UHMET 87-02, Department of Meteorology, University of Hawaii, Ho-